IIETA International Information and Engineering Technology Association
Advancing the World of Information and Engineering

Annales de Chimie - Science des Matériaux
Vol. 49, No. 5, October, 2025, pp. 489-495
Journal homepage: http://iieta.org/journals/acsm

Improving the Performance of Electroless Nickel Coatings Using TiN Nanoparticles on Gray Cast Iron

Mohammed Chekhyor*, Abdul Raheem Abid Ali

Metallurgical Engineering Department, College of Materials Engineering, University of Babylon, Babylon 51001, Iraq

Corresponding Author Email: mohammedsattar44@yahoo.com

https://doi.org/10.18280/acsm.490504

Received: 9 September 2025
Revised: 10 October 2025
Accepted: 17 October 2025
Available online: 31 October 2025

Keywords:
wear resistance, nano-particles reinforced, TiN-dispersion, non-electric Ni matrix, Vickers micro-hardness

ABSTRACT

Gray cast iron is widely valued in industry for its good mechanical performance and its ease of casting complex geometries; however, it exhibits only modest wear resistance and relatively low micro-hardness. In this research, Electroless nickel-phosphorus plating (ENP) was used to apply composite nickel-phosphorus coatings (Ni-P+TiN) to the surface of gray cast iron, aiming to enhance surface hardness and wear resistance. Sub-micron particles (280 nm) of titanium nitride are used in this research. Vickers microhardness, surface roughness, thickness of the coatings, EDS for coating layers, and wear rate measurements were used to characterize the substrate and the coated materials. The findings demonstrate that the coating is compact and uniform with varying thickness of the coatings when it is applied to gray cast iron. There is a 202.38% increase in the micro-hardness of the surface. In addition, surface roughness dropped about 28.82%, accompanied by a reduction in the wear rate percentage. The main objective of this research is to study the nickel-phosphorous electroless plating with additives of TiN particles on the micro-hardness and wear behavior of gray cast iron.

1. INTRODUCTION

Gray cast iron delivers high productivity at low cost and can reproduce complex forms, making it widely used across industry [1]. Like other metals and alloys, it undergoes various wear processes; in cast irons, frictional and dry-sliding wear dominate, so its wear resistance is typically good but not exceptional [2]. Gray cast iron is often used to make industrial parts like choke check valves, transport wheels, needle valves and cylinders that are used in oil and gas facilities and power plants where they are subjected to hard frictional conditions. They are always coming into touch with moving parts and small pieces of dirt that wear them down faster and shorten their life [3, 4]. Surface performance can be improved by electroless nickel (EN) deposition: Ni-P and Ni-P composite layers increase hardness and resist wear by forming a supersaturated solid solution. On heating, these coatings may precipitate Ni_3P, providing an additional hardness boost. However, as sliding wear progresses—and with increasing heat-treatment temperature—the hardness falls off rapidly. In comparative terms, the Ni-P-TiN layer shows superior hardness and markedly better wear resistance than either the Ni-P coating or the cast iron [5, 6].

Electroless Ni-P systems are rather extensively reinforced with different nano-particles such as TiN, SiC and also nano-alumina. TiN has been used in this work as the complex particle for co-deposition. The uptake of particles into the Ni-P layer is controlled by many parameters, including particle size and shape, relative density, surface charge and chemical stability, bath composition, agitation type, agitation strength, particle-matrix compatibility, and the component plating direction [7]. By choosing the suitable reinforcing media—from silicon carbides and ceramic fillers to fluoropolymers and alumina—composite coatings can be produced with specific functions [8-12].

Enhancing the influence of particles on the plating process mechanism results in an increased deposition rate, improved microstructure, and reduced reaction temperature [13]. In gray cast iron, the presence of graphite within the microstructure plays a key role in influencing how electroless nickel coatings adhere and perform. Interface defects are likely to form, increasing the risk of cracking because nickel is deposited on the substrate and not on the graphite. Uncoated areas promote the propagation of surface damage. This defect is not visible in steel. The shape of graphite has little effect compared to its concentration [1]. Surface wear resistance is controlled by both the matrix and the nature of graphite when other alloying elements are present. The size, quantity, distribution, and morphology of graphite in the alloy itself influence the friction pattern and mechanical strength. Changing the composition ratios of cast iron allows for better performance in applications that accommodate this change and through careful heat treatment [14-18]. The amount and appearance of graphite significantly influence the performance of the coating. Introducing minute amounts of nanoscale additives into the liquid metal drives the graphite to evolve from flake morphology toward compact, vermicular structures, while also modifying the matrix. The combined effect is a significant increase in durability against surface degradation [19, 20]. Park and Kim [21] studied the microhardness and cavitation

erosion resistance of electroless Ni plating on gray cast iron (FC250) in seawater, using an acidic solution. It was found that the wear resistance increased, and also that the micro-hardness increased with an increase in cavitation erosion resistance, noting that the plating time was 2 hours. Park and Kim [1] studied the electroless nickel plating characteristics of gray cast iron by adding lead nitrate at a controlled concentration. P content is (7%-8%) wt, which gives an enhancement in micro-hardness between (740-900) $HV_{0.1}$, which means it is enhanced by 42% when samples are plated. They indicated that wear resistance has increased. Moreover, every increase in hardness means increasing in wear resistance. Ortiz et al. [20] studied electroless Ni-P coatings on ductile cast iron (nodular cast iron) with a P content of 16% wt., which enhanced the micro-hardness by 53% after coating, as measured by $HV_{0.1}$. Additionally, Park and Kim [22], found an enhancement in microhardness by about 37.5% $HV_{0.1}$. Where was the study on gray cast iron (C: 3.33%, Si: 1.92%, Mn: 0.76%, P: 0.5%, S: 0.05%, Ni: 0.39%, Cr: 0.41%, Mo: 0.31%, Cu: 0.42%, Sn: 0.025%, Fe: balance) and P content was (8%-10%) wt. The time of electroless plating was 70 min. Moreover, the sample was then subjected to a 2-hour heat treatment at 250°C. They obtained a cavitation damage rate of 0.2 mg/h in their research. Hsu et al. [23] observed decreases in surface roughness after coating when using TiN powder, along with an increase in microhardness and wear resistance. The work focused on ADI containing (wt.%): 3.56 C, 2.83 Si, 0.22 Mn, 0.039 P, 0.008 S, and 0.042 Mg, with the remainder iron. The surface was engineered using an electroless Ni coating in parallel with a cathodic arc evaporation treatment. Experimental parameters were maintained at low pH throughout, a choice intended to improve deposition efficiency and the quality of the modified surface.

Previous studies included in this study did not use the same ratios as this study, nor did they use the same particle size. Furthermore, coating was not performed at the same time as this study. Previous studies were used to determine the method of application, the tests required for the coating layer, and the previous materials used as reinforcement. From this perspective, the nanomaterial to be added and the required proportions to be controlled were identified.

It's clear there's few studies about the TiN additives into Ni-P electroless plating. So that, in this research addition of nano-particles from TiN in the solution of Ni-P studied with different amounts.

This work aims to increase wear resistance and micro-hardness at different applications.

2. MATERIALS AND METHODS

The specimens used for EN plating were gray cast iron substrates, each machined to dimensions of 23 mm × 23 mm × 8 mm. The chemical composition of substrate (in weight percent) analysis by EDS on an SEM model (Axia-ChemiSEM) is (4.2% C, 2.9% Si, and the balanced metal is iron). The specimens were polished by using (SiC) paper from 180, 220, 400, 600, 800, 1000, 1200, 1500, up to grit #2000. Before the flexing electroless nickel plating process, all gray cast-iron specimens were cleaned by ultrasonic cleaning to completely remove surface contaminations such as greasy, dust particles, oxide films from the substrate surface to enhance coating adhesion. The specimens were degreased using analytical-grade acetone (≥ 99.5% purity) per ASTM B254-92, and then subjected to ultrasonic cleaning in acetone. Ultrasonic cleaning was carried out with a device model TB-30, at room temperature (25 ± 2°C). Preparation time is of 30 minutes per specimen. The samples were then gently washed with fresh deionized water and dried using filtered warm air. After ultrasonic cleaning, specimens underwent electro-cleaning to remove residual organic films, oxides, and polishing debris and to activate the metallic surface before electroless nickel deposition. A base solution (30 g/L Na_2CO_3 + 38 g/L NaOH) mixed with deionized water was used in the process. A rectangular 1 L glass beaker, a DC power supply set to 3V, a lead piece that worked as the cathode, and the specimen that worked as the anode were all parts of the cleaning cell that met ASTM B322-99. A temperature-regulated water bath maintained the electrolyte at 65 ± 2°C, ensuring proper emulsification and saponification of leftover oils. A magnetic stirrer was used for continuous agitation to make the ion concentration uniform around the metal sample, and also to avoid the accumulation of hydrogen bubbles on the surface of the sample at a rotation speed of 500 rpm. Electro-cleaning was performed for 2 minutes. Under these alkaline and anodic conditions, contaminants were electrochemically oxidized. This process resulted in fine gas evolution, which mechanically loosened tightly adhered films. Simultaneously, the alkaline solution chemically dissolved fatty acids and oxide residues. After the cleaning step in the solution was done, the samples were carefully taken out of the solution of cleaning. The samples were then rinsed with jet-distilled water to remove any remaining alkaline materials. Then warm air dried it. Electrochemical oxidation of contaminants occurred under these anodic and alkaline conditions. This process resulted in fine gas evolution, which mechanically loosened tightly adhered films. Simultaneously, the alkaline solution chemically dissolved fatty acids and oxide residues. After the cleaning step in the solution was done, the samples were carefully taken out of the solution of cleaning. They were washed well with jet-distilled water to get rid of any alkaline substances that were still there. then warm air dried it.

Table 1. The composition of EN plating bath

Substance	Concentration (g/L)
Nickel chloride	30
Sodium hypophosphite	10
Ammonium chloride	100
Titanium nitride	3,5,7,10
Sodium hydroxide	Adjust pH
Operating conditions	
pH	8-9
Temperature (°C)	88°C-90°C
Magnetic stirring (rpm)	200

Surface activation was carried out by acid pickling in 20 vol.% hydrochloric acid for 20 seconds, to remove oxides and to increases the adhesion force between the surface and the coating then washing it with deionized water and drying it according to ASTM B322-99, the sample is ready for coating. The exposed samples were then immersed in highly alkaline EN solution for 1 hour. Table 1 lists the EN bath composition, which was held constant during the process. Where the pH of EN bath was adjusted to a range of (8-9), this pH degree is achieved by continuing to add sodium hydroxide at room temperature and stopping the addition when the desired degree is reached. The bath consisted of a 1000 mL beaker, and the EN process was run for 1 hour with two samples. After

complete coating process, all specimen is put in small cup in tube furnace MTI-GSL1600X electrical tube furnace at 400°C for one hour.

Micro-Vickers hardness was quantitatively characterized on the surface and cross-section of uncoated gray cast-iron substrate and TiN nanoparticle-reinforced electroless nickel (EN) coatings. The measurements of hardness were done by using a TH-717 digital micro-Vickers hardness tester (Time Group Inc., China) equipped with an optical microscope and diamond pyramidal indenter having an apex angle of 136° between opposite faces. This test was carried out according to the requirements of ASTM E384-11 for micro-indentation hardness. Before evaluating the coated specimens, the device was calibrated with a certified reference block to ensure measurement accuracy. Environmental factors such as temperature was controlled at 25 ± 2 degree Celsius. Single-operator bias was eliminated as all measurements were conducted by a single operator. These works ensured the high reliability and comparability of the microhardness properties of the substrate of gray cast iron and the composite coatings of Ni-P-TiN. Five indentations were performed on each sample at randomly chosen, non-overlapping areas to prevent stress-field interference. The load applied was 50 g with a dwell period of ten sec., values selected to optimize indentation clarity and regulate surface deformation. The diagonal lengths of each indentation impression were measured accurately utilizing the integrated optical system at a magnification of 40×. The Vickers Hardness Number VHN is determined through the application of the standard Eq. (1) [24]:

$$VHN = 1.8544 \times (P/d^2) \quad (1)$$

In which P is the load being utilized in kilogram force and d is the indentation impression's mean diagonals in millimeters. The value of 1.8544 serves as a geometrical conversion coefficient that is based on the geometry of the indenter. For each indentation value the average between the five readings was taken and reported as the representative hardness value for the specimen. Additionally, the surface roughness of the coating and the substrate of the base is determined by taking six readings at different locations and calculating the average by using (HSR210) device. As for the wear test, it was carried out in the form of an overlay, and it was conducted on the sample before and after electroless coating, where different loads (5 and 10) N were taken for different times, where for each load the times were taken (10, 20, 30, 40) minutes, where combined for every specimen, the specific radius is 6 mm, where disk rotating speed is 250rpm and the radius is 6mm. The weight of the specimen was taken before starting work and after the end of each of the specified times. The specific wear rate of the specimen is calculated (ASTM G99) and is defined as in Eq. (2).

$$\text{Rate of the Wear (W.R.)} = \Delta W/2\pi.\,r.\,n.\,t.\,L \quad (2)$$

where,

W.R. = Rate of the Wear.

ΔW = the difference in weight loss (g) between the starting and ending weights of the specimen.

π= constant (3.14).

t = sliding time (min).

r = specimen radius (m).

n = disk rotation speed (rpm).

L= Load (N).

The thickness of coatings is done by utilizing scanning electron microscopy (VEGA3SBU).

3. RESULTS AND DISCUSSION

The average surface roughness and the average micro-hardness for the base and all samples are shown in Table 2.

Table 2. Compares the base and coatings samples in surface roughness and micro-hardness

Sample Code	Composition of Coating	Surface Roughness (μm)	Micro Hardness $HV_{0.05}$
Base	-	0.085	252
S1	Ni+3g TiN	0.4075	658
S2	Ni+5g TiN	0.0605	762
S3	Ni+7g TiN	0.0795	733
S4	Ni+10g TiN	0.405	741

The roughness measurements show that S1 and S4 became significantly rougher, driven by TiN nanoparticle clustering and poor surface dispersion, as shown in the Figure 1(a) for S1. The roughness decreased at S3, and the roughness dropped to its lowest point at S2, indicating a uniform and efficient distribution of nanoparticles, as shown in the Figure 1(b).

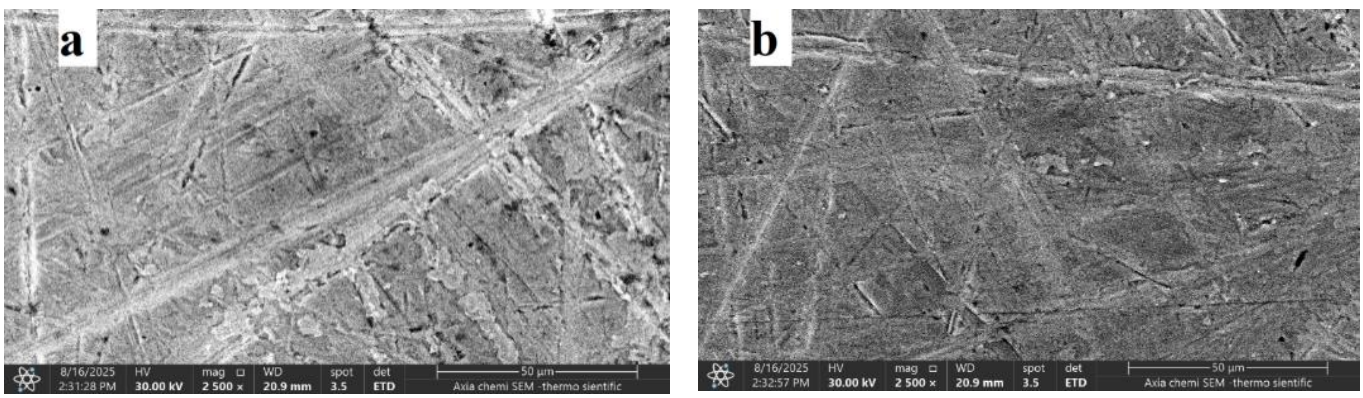

Figure 1. SEM photographs of the surface morphology at 2500x magnification force (a). S1 specimen; (b). S2 specimen

The highest hardness was found at S2, despite not containing the highest amount of TiN. This was due to the sub-micron particles being optimally distributed within the nickel matrix, resulting in strong bonding between the TiN and nickel without the formation of clumps or pores. S3 and S4 exhibited good hardness, although lower than that of S2, despite having a higher TiN content. This was due to the agglomeration of sub-micron particles due to the higher TiN content, which leads to microscopic defects and consequently weak cohesion. S2 achieved the best balance between high hardness and low roughness.

The measurements of wear rate before coating are shown in Table 3.

The uncoated base metal exhibits a higher wear rate than the coated samples at 5N and 10N loads, and this trend worsens at Summation (combined) Loads (5N + 10N). The Figure 2 shows the surface of the basic sample after the wear process for all loads used for all times.

Table 3. Wear rate of base specimen

Sample Code	Load (N)	Time (min)	Wear Rate ($\frac{g}{m \cdot N \cdot min}$)
Base	5	10	0
		20	1.8037e-6
		30	1.41470e-6
		40	1.22018e-6
	10	10	2.42975e-5
		20	1.24671e-5
		30	8.66508e-6
		40	6.87017e-6
	5+10	-	56.7384e-6

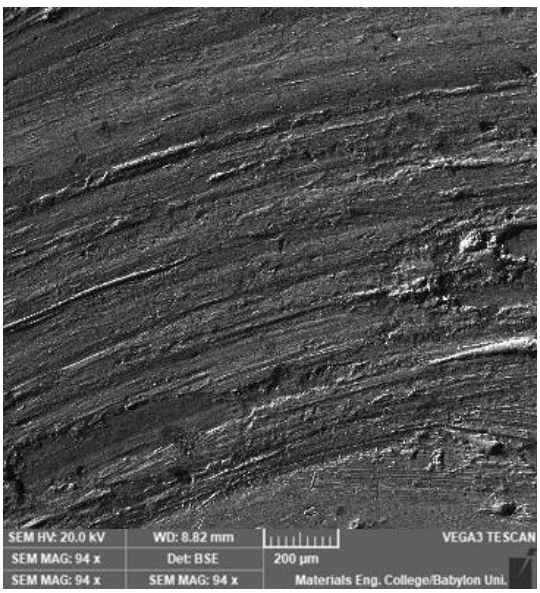

Figure 2. SEM analysis of the surface of bare sample after wear tests

After completing the electroless coating process on the samples at the required rates, a wear test was performed at an initial load of 5N on all samples. as shown in Table 4.

The results obtained in the table, shows the sample S2 gives the lowest wear rate, indicating that the resulting coating is more resistant to friction and wear under applied load, indicating high efficiency as shown in Figure 3. S4 came next and was close to S2. Although the wear rate was zero in the first half hour, the result was slightly less resistant, which may be attributed to variations in homogeneity. S3 had a relatively average performance, exhibiting good friction resistance but a higher wear rate compared to S2 and S4, suggesting that the added ratio was not effective. Finally, S1 exhibited a relatively high wear rate compared to the other samples.

Table 4. Wear rate of S1, S2, S3, and S4 with load 5N

Sample Code	Time (min)	Wear Rate ($\frac{g}{m \cdot N \cdot min}$)
S1	10	1.27323e-6
	20	1.16713e-6
	30	1.06103e-6
	40	7.95772e-7
S2	10	0
	20	1.06103e-7
	30	2.12206e-7
	40	2.65257e-7
S3	10	2.12206e-7
	20	2.12206e-7
	30	4.24412e-7
	40	6.36618e-7
S4	10	0
	20	0
	30	2.12206e-7
	40	4.77463e-7

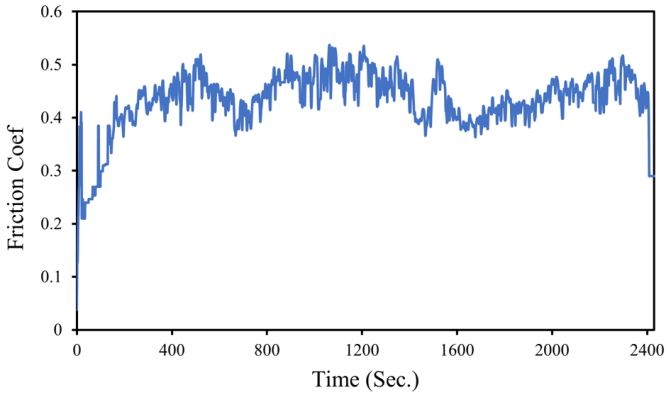

Figure 3. Coefficient of friction of S2 for 5N for 40 min

The work is completed in a superimposed manner using the 10N load for wear testing. as shown in Table 5.

Table 5. Wear rate of S1, S2, S3 and S4 with load 10N

Sample Code	Time (min)	Wear Rate ($\frac{g}{m \cdot N \cdot min}$)
S1	10	2.01595e-6
	20	1.11408e-6
	30	8.48824e-7
	40	8.22298e-7
S2	10	7.42721e-7
	20	3.71360e-7
	30	4.59779e-7
	40	4.50937e-7
S3	10	2.01595e-6
	20	1.90985e-6
	30	1.62691e-6
	40	1.32628e-6
S4	10	1.16713e-6
	20	6.89669e-7
	30	8.13456e-7
	40	1.03450e-6

The readings above show that, upon completion of the work using a 10N load, the wear rate was excellent for S2. This

indicates the effective surface structure in resisting friction and high mechanical resistance, thus outperforming the other samples as shown in Figure 4. S4 comes next, showing a clear improvement in effectiveness at high loads and outperforming the remaining samples. S1 and then S3 follow this.

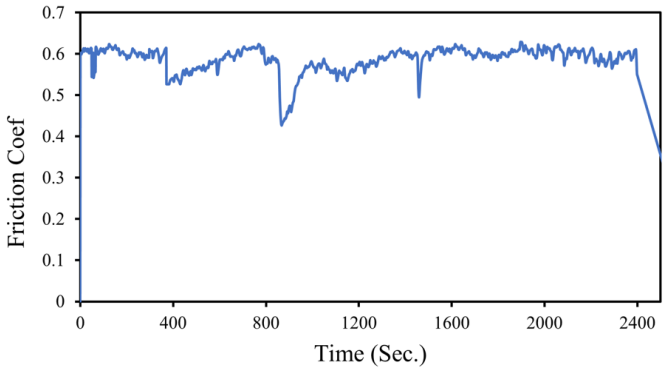

Figure 4. Coefficient of friction of S2 for 10N for 40 min

Table 6 shows the total wear rate at all loads and times. Table 6 displays the wear rate values for the four tested units (S1, S2, S3, and S4) under a combined mechanical load of 5 N + 10 N. The wear rate was measured in g/m.N.min to accurately and objectively determine the wear resistance performance of each sample.

Table 6. Wear rate of S1, S2, S3 and S4 with summation loads (5N+10N)

Sample Code	Wear Rate ($\frac{g}{m \cdot N \cdot min}$)
S1	5.09831e-6
S2	2.60836e-6
S3	8.36443e-6
S4	4.39442e-6

The results reveal that there are specific differences of wear resistance between the samples. Sample S2 obtained the minimum wear rate of 2.60836 × 10-6 g/m.N.min, which means highest resistance to wear at specific run conditions and as presented in Figure 5(a). Sample S4 followed with a wear rate of 4.39442 × 10-6 g/m.N.min, and then sample S1 with a wear rate of 5.09831 × 10^{-6} g/m.N.min. Sample S3 recorded the highest wear rate of 8.36443 × 10^{-6} g/m.N.min, as shown in Figure 5(b). Indicating the lowest wear resistance among the four coated specimens. Specimens can be ranked in terms of cumulative wear resistance performance (from the best to worst) as follows: S2→S4→S1→S3.

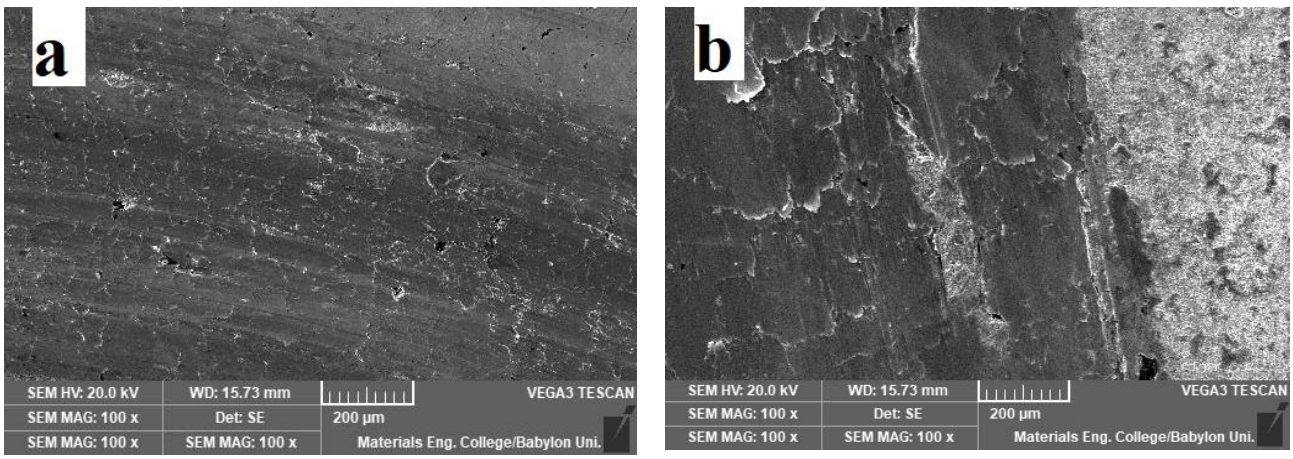

Figure 5. SEM photographs of the surface for coated specimens (a). Surface of S2 (b). Surface of S3

The results highlight that the structural properties or surface treatment applied to sample S2 played a significant role in reducing the wear rate, making it a promising candidate for applications requiring high wear resistance under combined loads.

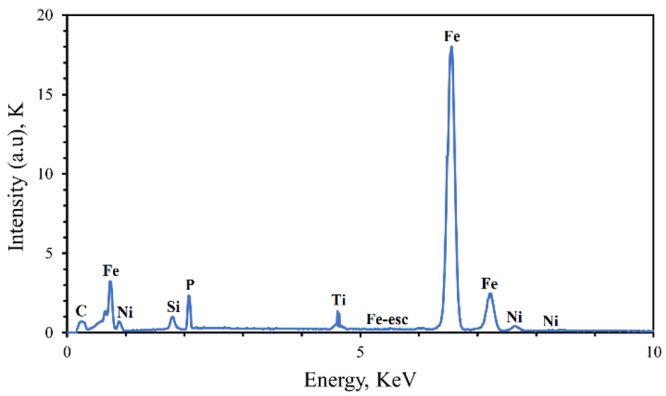

Figure 6. EDS charting results of S4

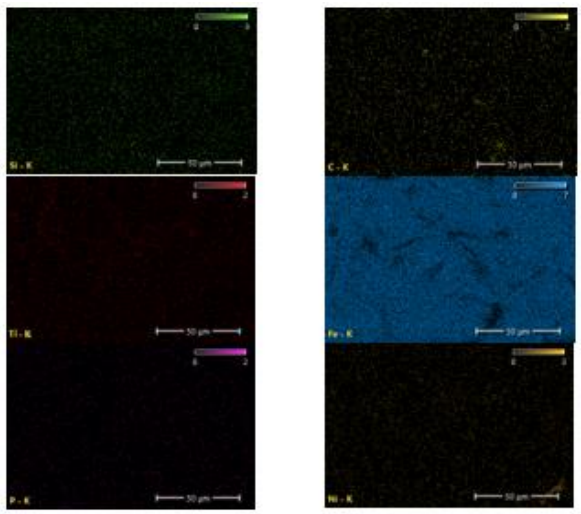

Figure 7. EDS distribution of elements in the coating of S4

EDS examination was performed on specimen 2 to show the

percentage of phosphor content and specimen 4 to see the distribution of elements in the coating layer, where it was found that the distribution of nanoparticles and deposited elements on the surface is random, as shown in Figures 6 and 7, and the percentage of phosphorus was found to be 3.7%.

This clearly indicates the optimal amount is 5 g of TiN, at which surface roughness, microhardness, and wear rate achieved the best values. The increase in microhardness is attributed to the appropriate addition of ceramic material (TiN) to the solution.

Lastly, the thicknesses of the coating layer for weights 3 g, 5 g, 7 g, and 10 g measured were 3.016 µm, 9.94 µm, 2.48 µm, and 7.85 µm. The highest thickness was obtained in specimens, with a value of 9.94 µm, as proved in Figure 8.

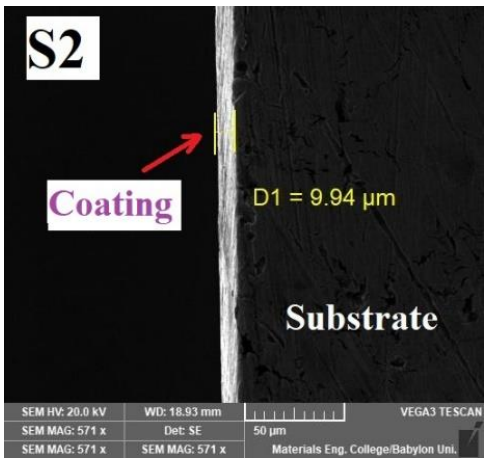

Figure 8. SEM picture for cross-section of coated specimen S2

4. CONCLUSION

Results indicate that TiN nanoparticle additions to Ni-P electroless coatings substantially enhance gray cast iron's surface response. The best solution was found to be the one containing 5 grams of titanium nitride, and the results of this were demonstrated in Sample 2, where the Vickers hardness test result was more than 200%. The coated surface was more homogeneous, and the wear rate was significantly reduced under medium and high loads. These improvements were achieved due to the homogeneous distribution of titanium nitride particles in the nickel phosphorus matrix, which in turn strengthens the coating and reduces agglomeration, which in turn leads to further defects. Based on the results obtained, the particle distribution indicates that nanocomposite coatings are the best choice for coating parts found in applications that deal with high friction rates (high wear rates) on a regular basis. Therefore, to increase the operational life of parts subject to wear in long-term applications, slip tests must be performed on them to determine the changes that occur in the surface and the resulting effect on wear resistance.

ACKNOWLEDGMENT

We thank the Deanship of the College of Materials Engineering and the Head of the Department of Metallurgical Engineering for allowing us to use the college laboratories to complete our work requirements.

REFERENCES

[1] Park, I.C., Kim, S.J. (2019). Effect of lead nitrate concentration on electroless nickel plating characteristics of gray cast iron. Surface and Coatings Technology, 376: 2-7. https://doi.org/10.1016/j.surfcoat.2018.12.084

[2] Rao, S.V., Venkataramana, M., Kumar, A.C.S. (2021). Friction and dry sliding wear properties of compact graphite iron at room temperature and 100°C. Materials Today: Proceedings, 45: 3250-3254. https://doi.org/10.1016/j.matpr.2020.12.385

[3] Parkinson, R. (1997). Properties and Applications of Electroless Nickel (Vol. 37). Toronto: Nickel Development Institute.

[4] Sudagar, J., Lian, J., Sha, W. (2013). Electroless nickel, alloy, composite and nano coatings-A critical review. Journal of Alloys and Compounds, 571: 183-204. https://doi.org/10.1016/j.jallcom.2013.03.107

[5] Zarebidaki, A., Akbarpour, M. (2024). Corrosion and wear behavior of electroless Ni-P-Cu coatings containing 8 and 18 wt% Cu. Surface and Coatings Technology, 492: 131228. https://doi.org/10.1016/j.surfcoat.2024.131228

[6] Kaleicheva, J.A., Karaguiozova, Z.K. (2018). Electroless composite nickel coatings strengthening with TiN nanoparticles plated on ductile cast iron. Materials Science Forum, 919: 52-58. https://doi.org/10.4028/www.scientific.net/MSF.919.52

[7] Li, Q., Ni, M., Huang, W. (2024). Microstructure and mechanical properties of electroless Ni-P-Si3N4-TiN composite coatings. Materials Science and Technology, 40(8): 571-580. https://doi.org/10.1177/02670836231219188

[8] Chintada, V.B., Uppada, S., Gurugubelli, T.R., Koutavarapu, R., Alharthi, S.S. (2025). Impact of electroless ZnO, SiC, and Al2O3 reinforced Ni-P coatings on brake pad properties. iScience, 28(6): 112680. https://doi.org/10.1016/j.isci.2025.112680

[9] Ahmad, M., Samra, A.S., Habib, S., Kahraman, R., et al. (2025). Mechanical properties and corrosion resistance of electroless deposited Ni-P-Y2O3 nanocomposite coatings for industrial applications. Scientific Reports, 15(1): 26707. https://doi.org/10.1038/s41598-025-12319-6

[10] Badiee, F., Arabian, D., Jamali, H., Torkian, S. (2025). Investigation of wear behavior of Ni-P/Ni-B-CeO2 composite coating. Results in Surfaces and Interfaces, 19: 100482. https://doi.org/10.1016/j.rsurfi.2025.100482

[11] Malathi, M., Mabel, J.H., Easwaramoorthy, D., Rajendran, R. (2024). Ni-P SiC composite coatings on piston rings by plate and bumper technique and its tribological properties. Surface Engineering, 40(11-12): 1063-1078. https://doi.org/10.1177/02670844241293510

[12] Gul, H., Usta, I. (2023). Effect of alumina concentration on morphology, wear, and corrosion: Electroless Ni-W-P/Al2O3 composite coatings on aluminum surfaces. Journal of Materials Engineering and Performance, 32(13): 6107-6122. https://doi.org/10.1007/s11665-023-08184-x

[13] Tulinski, E.H. (1994). Mass finishing. In Surface Engineering. ASM International, pp. 118-125. https://doi.org/10.31399/asm.hb.v05.a0001234

[14] Hase, A. (2019). Visualization of the tribological

behavior of graphite in cast iron by in situ observations of sliding interfaces. Tribology International, 138: 40-46. https://doi.org/10.1016/j.triboint.2019.05.031
[15] Panneerselvam, S., Putatunda, S.K., Gundlach, R., Boileau, J. (2017). Influence of intercritical austempering on the microstructure and mechanical properties of austempered ductile cast iron (ADI). Materials Science and Engineering: A, 694: 72-80. https://doi.org/10.1016/j.msea.2017.03.096
[16] Srivastava, R., Singh, B., Saxena, K.K. (2020). Influence of S and Mn on mechanical properties and microstructure of grey cast iron: An overview. Materials Today: Proceedings, 26: 2770-2775. https://doi.org/10.1016/j.matpr.2020.02.577
[17] Wollmann, D., Pintaude, G. (2021). Tribological performance of high-strength cast iron in lubricated contact containing carbon black. Wear, 476: 203743. https://doi.org/10.1016/j.wear.2021.203743
[18] Lyu, Y. (2019). Abrasive wear of compacted graphite cast iron with added tin. Metallography, Microstructure, and Analysis, 8(1): 67-71. https://doi.org/10.1007/s13632-018-0504-8
[19] Wang, Y., Pan, Z., Wang, Z., Sun, X., Wang, L. (2011). Sliding wear behavior of Cr–Mo–Cu alloy cast irons with and without nano-additives. Wear, 271(11-12): 2953-2962. https://doi.org/10.1016/j.wear.2011.06.015
[20] Ortiz, N., González-Parra, J.R., Olaya, J., Agredo, D., et al. (2024). Morphological and corrosion characterization of electroless Ni-P coatings deposited on ductile iron. Coatings (2079-6412): 14(10): 1317. https://doi.org/10.3390/coatings14101317
[21] Park, I.C., Kim, S.J. (2019). Effect of stabilizer concentration on the cavitation erosion resistance characteristics of the electroless nickel plated gray cast iron in seawater. Surface and Coatings Technology, 376: 31-37. https://doi.org/10.1016/j.surfcoat.2018.08.098
[22] Park, I., Kim, S. (2019). Cavitation erosion damage characteristics of electroless nickel plated gray cast iron. Acta Physica Polonica A, 135: 1018-1022. https://doi.org/10.12693/APhysPolA.135.1018
[23] Hsu, C.H., Huang, K.H., Chen, Y.T., Ho, W.Y. (2013). The effect of electroless Ni-P interlayer on corrosion behavior of TiN-coated austempered ductile iron. Thin Solid Films, 529: 34-38. https://doi.org/10.1016/j.tsf.2012.05.050
[24] Cámara, F., Bellatreccia, F., Ventura, G. D., Gunter, M.E., Sebastiani, M., Cavallo, A. (2012). Kircherite, a new mineral of the cancrinite-sodalite group with a 36-layer stacking sequence: Occurrence and crystal structure. American Mineralogist, 97(8-9): 1494-1504. https://doi.org/10.2138/am.2012.4033

NOMENCLATURE

C	Concentration in EN bath ($g \cdot L^{-1}$)
HV	Vickers microhardness (dimensionless)
L	Normal load in pin-on-disk test (N)
n	Disk rotation speed (rpm)
pH	Acidity/alkalinity of EN bath (dimensionless)
r	Wear track radius (m)
Ra	Surface roughness (μm)
T	Temperature (°C)
t	Sliding time (min)
W.R.	Specific wear rate ($g \cdot m^{-1} \cdot N^{-1} \cdot min^{-1}$)